System-Level Dynamic Analysis of Alkaline Water Electrolysis Coupled to Wind Power Fluctuations

Su Lim[a] and Young Duk Lee[b]

[a] Department of Energy Engineering, Korean Institute of Energy Technology (KENTECH), Naju-si, Republic of Korea, su.lim@kentech.ac.kr
[b] Department of Energy Engineering, Korean Institute of Energy Technology (KENTECH), Naju-si, Republic of Korea, ydlee@kentech.ac.kr, CA

Abstract:
The rapid expansion of variable renewable energy is increasing the need for flexible power-to-hydrogen systems that can operate safely under fluctuating input conditions. Green hydrogen is attracting growing attention as a long-duration energy carrier, and alkaline water electrolysis (AWE) remains one of the most mature options for MW-scale hydrogen production. However, direct coupling of AWE with renewable energy can drive the system into low-load operation and frequent transient conditions, where thermal imbalance, gas crossover, and system level dynamics become important. Therefore, dynamic modeling is essential to evaluate dynamic behavior and define a practical operating envelope beyond steady-state performance.
In this study, a dynamic model of a 2.3 MW-scale AWE system was developed by integrating the stack and major balance-of-plant (BOP) units, including the electrolyte recirculation loop, gas–liquid separators, cooling section, and a simplified hydrogen purification section. The model was used to analyze thermal management, hydrogen-in-oxygen (HTO)-based safety behavior, and ramp-rate-constrained current response. The thermal analysis showed that the required electrolyte flow strongly depends on both operating load and allowable temperature rise across the stack. The HTO analysis indicated that pressure has a stronger influence than temperature on the safety limit under low-current-density operation, allowing a safe operating region to be identified based on the 2% threshold.
Wind-coupled dynamic simulations were then carried out using actual wind power data. Under high wind conditions, the system maintained stable temperature, separator level, and pressure behavior, while HTO remained well below the safety limit, producing 863 kg of hydrogen over 24 h. Under low wind conditions, the system operated predominantly in the low-load region, where HTO remained above 1% but below the safety threshold, clearly demonstrating the importance of defining an appropriate operating load range in AWE systems. Overall, the proposed framework provides a useful basis for evaluating the dynamic operability and safety of MW-scale AWE systems under renewable-driven operation.

Keywords:
Alkaline water electrolysis; Dynamic; Hydrogen production; Renewable energy; Wind power.

1. Introduction

The global transition toward clean energy has gained strong global momentum in response to carbon neutrality goals. As a result, renewable electricity, particularly wind and solar energy, is expanding rapidly. The IEA projects that almost 4,600 GW of new renewable capacity will be added between 2025 and 2030 [1]. However, this rapid expansion also introduces a critical challenge: curtailment, which occurs when the power system cannot absorb all available renewable electricity. As the share of renewables increases, the risk of curtailment rises, highlighting the need for flexible solutions such as energy storage. In this context, hydrogen is attracting increasing attention as a versatile energy carrier, and water electrolysis offers a promising pathway to convert surplus renewable electricity into hydrogen for long-duration energy storage and improved renewable utilization. Among water electrolysis technologies, AWE remains one of the most mature and commercially established options for large-scale hydrogen production. Its industrial relevance is illustrated by large projects such as the Sinopec Kuqa plant, which has a total installed electrolyzer capacity of 260 MW [2]. However, renewable-coupled AWE operation presents challenges beyond steady-state performance. Under fluctuating

power input, the system must accommodate not only variations in current and voltage, but also dynamic changes in temperature, pressure balance, electrolyte circulation, and gas purity. These coupled dynamics are especially important in AWE because the liquid-electrolyte system requires coordinated stack to the balance-of-plant (BOP) operation, including gas–liquid separation, electrolyte management, cooling, and safe control against gas crossover. To address these issues, this study develops a dynamic AWE model from the stack to the BOP level for a renewable-driven AWE system. The objective is to evaluate the dynamic response of the system under variable power input and to identify the operating conditions required for safe and efficient hydrogen production.

1.1. Literature review and research gap

Previous studies have examined the dynamic behavior of AWE systems. In particular, dynamic system-level models have been developed to analyze thermal response, gas crossover behavior, and safe operating ranges under renewable-coupled operation. Wang et al. developed a dynamic system-level model for a wind-powered AWE system considering both thermal behavior and gas purity. Using the gas purity model, they identified a stable operating load range under varying temperature and pressure conditions. They further compared before-stack and after-stack temperature-control strategies under fluctuating wind-power input, showing that after-stack control provided better thermal stability and improved system efficiency by reducing cooling-system power consumption [3]. Sakas et al. developed and validated a dynamic system-level model of a 3 MW, 16 bar pressurized AWE plant using real operational data. A key contribution of the study is the introduction of a shunt-current-related heat-generation term to improve agreement with measured temperature dynamics, highlighting the importance of shunt currents in MW-scale thermal behavior and efficiency loss. The model also adopted a semi-empirical U–I fitting approach rather than a fully mechanistic electrochemical formulation, enabling closer agreement with plant data. Overall, the study provides a valuable industrial-scale reference for dynamic modeling of pressurized AWE systems [4]. Yin et al. developed 1-D electrolyzer to capture spatially distributed temperature and voltage behavior. Their study is notable in that HTO was modeled through diffusion, pressure driven convection, and electrolyte recirculation. The results showed that increasing electrolyte flow improves temperature uniformity but can simultaneously increase HTO through enhanced dissolved-gas mixing. They further reported different Multiphysics timescales, showing that current occurs on the order of seconds, whereas temperature and HTO evolve on the order of minutes [5]. Degradation and ramp-rate can also be a relevant factor in dynamic operation. Previous studies suggest that repeated load fluctuations accelerate performance decrement and reduce stack lifetime, indicating that degradation can act as a practical long-term constraint. Commercial comparisons have shown an efficiency degradation rate on the order of 1 %/year for AWE system degradation rate [6]. Taranin et al. have shown that the transient response of electrolyzers may be influenced by ramp-rate limitations associated with stack-level, as well as plant-level constraints including converter response, cooling requirements, pressure control, and safety constraints [7].

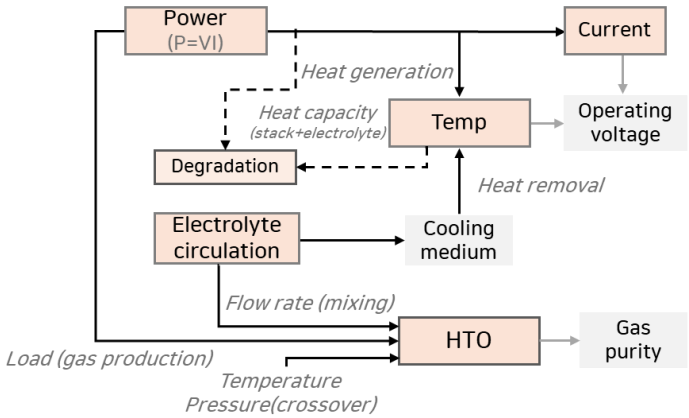

Figure. 1. *Dynamic interaction of the AWE system*

Previous studies have identified several key dynamic constraints in AWE, including electrolyte circulation, gas crossover, temperature variation, and multi-timescale response (Figure 1). Based on these insights, this study develops a stack-to-BOP dynamic framework for a MW-scale AWE system by integrating major process units

such as the gas–liquid separator, electrolyte recirculation loop, and heat exchanger. The analysis focuses on thermal management, HTO-based safety, ramp-rate-constrained response, and wind-coupled hydrogen production under both high- and low-wind conditions.

2. AWE dynamic modeling methodology

2.1. AWE system dynamic constraints modelling

Unlike steady-state model, dynamic analysis is required to capture dynamic response of the AWE system under variable power input. Power fluctuations, such as wind power, affect not only the operating current and voltage, but also the stack temperature, electrolyte circulation, and gas purity, which in turn determine the feasible operating range and safety of the system. In addition, because the AWE system employs a liquid electrolyte, dynamic considerations at the balance of plant (BOP) level are also important, including gas–liquid separation, electrolyte circulation, make-up water supply, and cooling management. Therefore, in this study, the previously developed rigorous electrochemical model was extended by incorporating dynamic constraints associated with thermal and gas purity behaviors of the AWE system [8]. The detailed electrochemical model of the AWE system employed in this study is described in Appendix A.

2.1.1. Thermal model

A lumped stack model was employed to describe the dynamic temperature response of the AWE stack. The thermal model was determined as expressed in Eq. (1). The thermal model was governed by three major terms: electrochemical heat generation (Q_{gen}), heat removal by electrolyte recirculation (Q_{lye}), and heat exchange associated with the generated gases (Q_{gas}).

$$C_{stack}\frac{dT_{out}}{dt} = Q_{gen} - Q_{lye} - Q_{gas}, \qquad (1)$$

The electrochemical heat generation term represents the net heat generation during electrolysis and was calculated form difference of operating voltage and thermoneutral voltage [9], [10], as given in Eq. (2). The electrolyte recirculation term accounts for the heat removed from the stack by the circulating electrolyte mass flow rate, which acts as the cooling medium in the system. As shown in Eq. (3), this term depends on the electrolyte mass flow rate, specific heat capacity, and the temperature difference in AWE stack. The heat removal with gases term was included to account for heat carried by the generated hydrogen and oxygen gases, as expressed in Eq. (4). Since the reaction product gases are generated throughout the stack, they were assumed to be formed at the average stack temperature and heated to the outlet temperature before leaving the stack. The total heat capacity of the stack was calculated from the thermal capacitance of the major stack components, as given in Eq. (5) [4]. Heat loss to environment is neglected in this study.

$$Q_{gen} = N_{cell}\, j_{op}\, A_{cell}\, (V_{cell} - V_{tn}), \qquad (2)$$

$$Q_{lye} = \dot{m}_{lye}\, c_{p,lye}\, (T_{out} - T_{in}), \qquad (3)$$

$$Q_{gas} = \dot{m}_{H_2}\, c_{p,H_2}\, \left(T_{out} - T_{avg}\right) + \dot{m}_{O_2}\, c_{p,O_2}\, (T_{out} - T_{avg}), \qquad (4)$$

$$C_{stack} = N_{cell}\, A_{cell}\, \left(2\, \rho_{ele}\, c_{p,ele}\, \delta_{ele} + 2\, \rho_{PTL}\, c_{p,PTL}\, \delta_{PTL} + \rho_{sep}\, c_{p,sep}\, \delta_{sep} + 2\, \rho_{lye}\, c_{p,lye}\, \delta_{lye}\right), \qquad (5)$$

2.1.2. Gas purity model

The gas purity model was used to track HTO, which is key safety indicator in AWE system under dynamic operation. As described by Eq. (6), the HTO level is determined by the combined effects of diffusion , electrolyte circulation, and convection-related crossover [5]. In AWE system, HTO is limited to 2 % as a safety shutdown threshold, which corresponds to approximately 50% of the lower explosion limit [3], [11]. Under low-load operation, HTO can increase more easily because gas production rate decreases while crossover term does not decline proportionally [3]. Therefore, gas purity becomes particularly important in the low-load operating region and can be an important factor in defining the feasible operating range of the AWE system. To account for HTO behavior, the empirical correlation proposed by Sánchez et al. was used in the simulation [12]. In case of oxygen-in-hydrogen (OTH), OTH was neglected in this study because its concentration is much lower than that of HTO and remains well below the safety constraints.

$$HTO(t) = \frac{N_{H_2}^{impurity}}{N_{O_2}},\ N_{H_2}^{impurity} = N_{H_2}^{diffusion} + N_{H_2}^{convection} + N_{H_2}^{mixing}, \qquad (6)$$

2.1.3. Current-density response constraint

In AWE systems, rapid changes in operating load may be limited by stack protection requirements, electrochemical response, and system-level delays. Therefore, a ramp-rate limit can be introduced to restrict the rate of change in operating load and maintain safe and feasible operating conditions [7]. In this study, the concept of a ramp-rate limit was introduced to prevent the current density from changing instantaneously. This formulation provides a simple way to account for the finite current-density response that may arise during dynamic operation, as expressed in Eq. (7).

$$\frac{dj_{ramp}}{dt} = \min\left(max\left(\frac{j_{op}-j_{ramp}}{\tau_j}, -R_{down}\right), R_{up}\right), \quad (7)$$

2.2. MW-scale AWE system configuration

To analyze MW-scale hydrogen production under dynamic operating conditions, a 2.3 MW AWE system was developed. The system consists of an AWE stack, an electrolyte circulation loop, a make-up water loop, gas–liquid separators at the anode and cathode, a cooling unit including a heat exchanger, and a hydrogen purification unit. The overall process configuration is described in Figure. 2.

The system was designed based on steady-state operating conditions, which were subsequently extended to dynamic simulations. Under the design point, the system operates at a power input of 2 MW, with an electrolyte flow rate of 3000 kmol/h using a 30 wt% KOH solution. The operating temperature and pressure are maintained at 75 °C and 7 bar, respectively. The stack operates at an average cell voltage of 1.83 V and a current density of approximately 3500 A/m², resulting in a hydrogen production rate of about 40 kg/h. The overall system efficiency is estimated to be approximately 80% based on the higher heating value of hydrogen. The parameter for determining the stack operating voltage is summarized in Appendix B. The system was scaled up using an identical building block approach, assuming consistent electrochemical performance, by increasing the cell area and the number of cells.

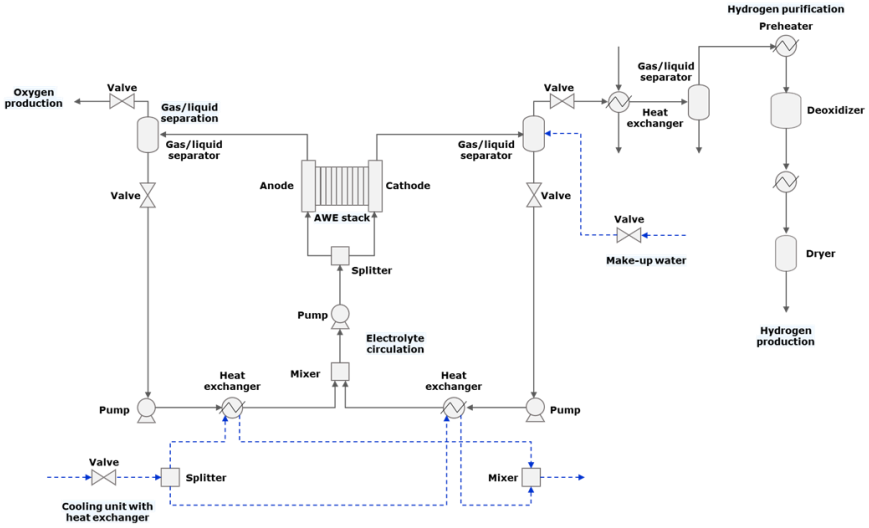

Figure. 2. *Dynamic AWE system configuration*

2.2.1. Hydrogen production process

2.2.1.1. Gas–liquid separation

To separate the generated hydrogen and oxygen from the AWE stack, gas–liquid separators were placed on the anode and cathode sides, respectively. The separator volume was determined based on the liquid-phase volumetric flow entering the gas–liquid separator, as obtained from the simulation. A liquid hold up time of 10 min was assumed. In addition, a separator length to diameter ratio of 3:1 was applied [13], [14]. Based on these assumptions, the separator dimensions were determined as 1.4 m in diameter and 4.3 m in height.

2.2.1.2. Electrolyte recirculation and cooling

The electrolyte leaving the gas–liquid separators was recirculated to the stack through the electrolyte loop. To maintain the stack temperature within the desired operating range, a cooling unit was included in the recirculation line to remove excess heat from the circulating electrolyte through heat exchanger. Water consumed during electrolysis was continuously replenished through a make-up water stream in order to maintain the electrolyte inventory during operation.

2.2.2. Hydrogen purification process

The hydrogen stream from the AWE cathode outlet contains residual impurities, primarily oxygen and moisture. To meet ISO 14687 hydrogen quality standard [15], a purification step was configured: a preheater, a deoxidizer, and a chiller with separator, and a dryer. In the deoxidizer, residual oxygen is removed via catalytic recombination. The subsequent chiller and separator reduce bulk moisture through cooling and condensation. At the chiller outlet, the hydrogen stream composition was estimated at approximately 99.5% H2 and 0.5% moisture, indicating that an additional drying step is required to achieve the target moisture content below 5 ppm. For the final drying step, a fixed bed dryer process was selected due to producing very dry products. The dryer was modeled with a single-component moisture adsorption objective, with Zeolite 4A selected as the adsorbent. Zeolite is among the most widely used adsorbents for moisture removal, particularly in air drying and fuel ethanol dehydration processes. Most existing moisture adsorption models have been developed either for air drying or fuel ethanol dehydration [16], [17], [18]., and experimental data under AWE stream conditions are not available. For the adsorption equilibrium, the isotherm model proposed by Gorbach et al. [16] for water adsorption on Zeolite 4A was adopted and implemented, as the model objective and operating conditions are consistent with those of this study. The dryer was modeled targeting single-component moisture removal. The carrier gas (hydrogen) was assumed to have negligible interaction with the zeolite adsorbent, since hydrogen molecules are not significantly adsorbed on Zeolite 4A and therefore do not compete with water molecules for adsorption sites.

2.2.3. Control strategy

To ensure stable and safe operation of the AWE system under dynamic conditions, controllers were implemented for the gas–liquid separation, electrolyte concentration, and thermal management. In the gas–liquid separation section, two types of controllers were used to regulate separator pressure and liquid level, and each controller was applied to both the anode and cathode sides. An additional controller was employed to maintain the electrolyte concentration at 30 wt% KOH by adjusting the make-up water flow rate to compensate for the water consumed during electrolysis. The cooling-water flow controller was used to regulate the thermal condition of the AWE system. In this study, the cooling-water flow rate was manipulated to maintain a constant stack inlet temperature.

2.3. AWE dynamic model validation

The model of AWE stack was validated using experimental data obtained from a 20 kW-scale system. The simulated stack voltage was then directly compared with the experimentally measured voltage over time. As shown in Figure. 3, the model reproduces the overall ramp-up trend of the experimental response. The comparison between the model and experimental data was evaluated using the mean absolute percentage error, which was found to be 0.71%.

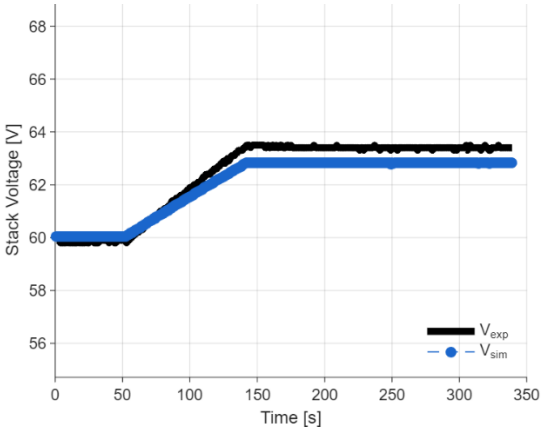

Figure. 3. *AWE dynamic validation*

3. Dynamic response characteristics

3.1. AWE system dynamic response

Figure. 4 (a) presents the thermal balance map of the AWE stack under the assumed electrolyte temperature of 70 °C at the inlet and 75 °C at the outlet. The black line indicates the minimum electrolyte flow required to satisfy the thermal balance condition under an assumed 5 °C temperature rise across the stack. As the load increases, the required electrolyte flow also increases. The region to the right of the black line corresponds to heating dominant conditions, where heat generation exceeds heat removal by the electrolyte, whereas the region to the left corresponds to cooling dominant conditions. Figure. 4(b) shows the required electrolyte flow for different electrolyte temperature rises across the stack. As the allowable temperature rise increases, the required electrolyte flow decreases over the entire load range. This indicates that the electrolyte flow requirement is strongly dependent on the assumed stack temperature difference and operating load.

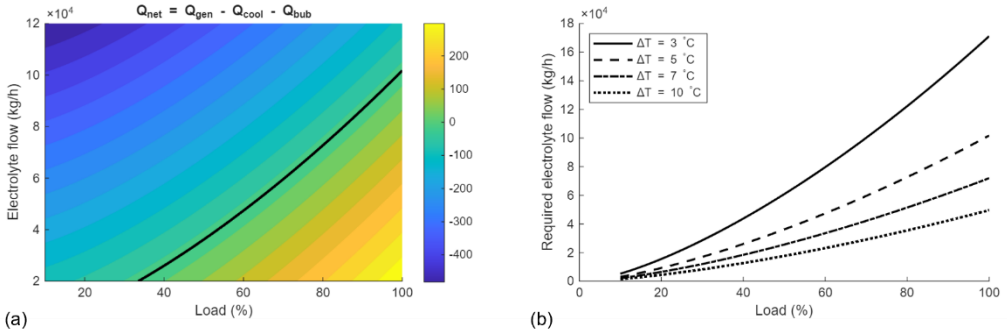

Figure. 4. *Thermal model analysis a) thermal map of net heat generation, b) required electrolyte flow*

Based on the empirical correlation proposed by Sánchez et al. [12], the HTO level was estimated as a function of temperature and pressure at a fixed current density (Figure. 5 (a)). Since HTO can more easily approach its safety limit under low current density operation [3], where hydrogen production is relatively low, the analysis was carried out at a low current density of 800 A/m². The contour map indicates that the HTO threshold was reached at 21.38 bar at 60°C, 21.37 bar at 70°C, and 21.28 bar at 80°C. This suggests that the allowable pressure slightly decreases with increasing temperature. However, pressure has a more dominant effect than temperature under these conditions. In Figure. 5 (b), the region below the black 2% limit line corresponds to the safe operating region.

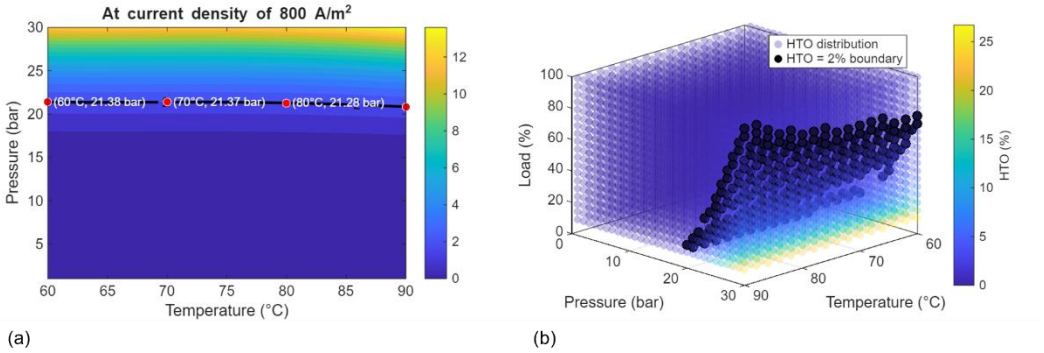

Figure. 5. *HTO analysis a) contour map at 800 A/m², b) distribution with operating conditions*

Figure. 6 shows the current-density transition under prescribed ramp-rate limits of 20%, 30%, and 40% per minute. As a result, the current density did not change instantaneously to the new setpoint even when a step input was applied. A higher limit led to a faster approach to the target value. These results indicate that the rate of change constraint smooths the current response under dynamic operation and prevents abrupt changes.

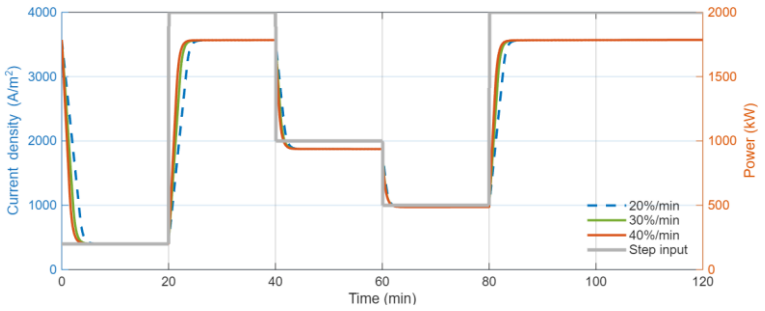

Figure. 6. *Dynamic rated current density*

3.2. Single-bed adsorption model

A single-bed adsorption model was applied to evaluate the moisture removal performance. The feed flow rate was set to 15 kmol/h, with an inlet composition of 99.5% H_2 and 0.5% H_2O after the upstream purification units. The bed diameter was fixed at 0.2 m, while the bed length was varied from 0.4 to 1.6 m. The breakthrough time was defined as the time at which the outlet moisture concentration exceeded 5 ppm. Figure 7. (a) showed the outlet breakthrough behavior for the case with a bed length of 1 m. As moisture breakthrough occurred, the outlet H2 mole fraction gradually decreased. Figure 7. (b) presented the water loading at different axial positions in the bed. The inlet region reached saturation earlier, indicating the propagation of the moisture adsorption front through the bed. The effect of bed length on the hydrogen purification duration was also evaluated. As the bed length increased, the breakthrough time increased from 200 s at 0.4 m to 5025 s at 1.6 m (Table. 1). This result indicates that increasing the bed length delays moisture breakthrough by increasing the available adsorption capacity and gas–solid contact time.

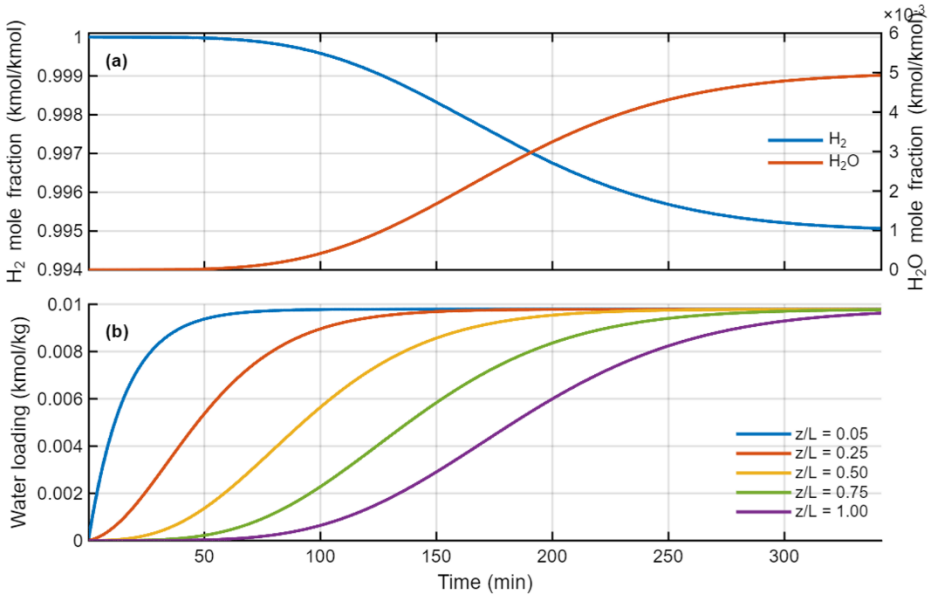

Figure. 7. *Single-bed adsorption a) outlet breakthrough curve for the 1 m bed, b) water loading at different axial positions*

Table 1. *Effect of bed length on five-nine hydrogen breakthrough time*

Bed length (m)	Breakthrough time (s)
0.4	200
0.6	550
0.8	1485
1	2375
1.2	3235
1.4	4125
1.6	5025

4. Wind-coupled AWE dynamic simulation

4.1. Hydrogen production process dynamic response

The dynamic response of hydrogen production was analyzed using real-time wind power data obtained from the Yeonggwang Baeksu Wind Farm in South Korea. The applied dataset consists of wind power output with a temporal resolution of 10 min, and an AC/DC conversion efficiency of 95% was assumed to determine the power input to the AWE system. In the wind-coupled analysis, current-density input dynamics were not implemented. For each wind profile, a representative one-day period was extracted, and continuous data points at 10-min intervals (600 s) were used for the dynamic simulation, while linear interpolation was applied within the dynamic simulation to ensure continuous system response. The simulation results were recorded at 0.5-minute intervals.

4.1.1. Dynamic response under high wind power conditions

Figure. 8 presents the dynamic response of the AWE system under high wind power input over a 24-hour period. As shown in Figure. 8 (a), the wind power fluctuates with an average value of approximately 1700 kW. The stack temperature in Figure. 8 (b) shows a gradual increase from 72 °C to 78 °C, while the average stack temperature remains around 75 °C. Despite rapid variations in wind power, the temperature profile remains stable without abrupt changes. As shown in Figure. 8 (c), the cooling water flow rate is adjusted to maintain stack inlet temperature at 70 °C. The cooling water flow rate generally follows the variation in stack heat generation. The HTO value shown in Figure. 8 (d) remains well below the safety threshold of 2% throughout the entire operation. Although slight spikes are observed during transient conditions, particularly under rapid load changes, the system operates within a safe regime. This indicates that at high load operation, the increased gas production effectively suppresses gas crossover, maintaining low HTO level. The make-up water stream shows negligible variation due to the relatively short simulation period. Figure 9 shows the dynamic behavior of the gas–liquid separation section under high wind power input, indicating stable operation at high load. As shown in Figure. 9 (a) and (b), both the anode and cathode separator levels remain nearly constant at approximately liquid level of 2.7m, indicating that the separator holdup is well maintained despite variation in operating conditions. The level deviation remained approximately 0.1 cm. The separator pressures shown in Figure. 9 (c) and (d), also exhibit stable behavior, remaining to 7 bar throughout the operation. The pressure deviation remained to approximately 0.03 bar. During this period, a total of 863 kg of hydrogen was produced, corresponding to an average production rate of 35.96 kg/h.

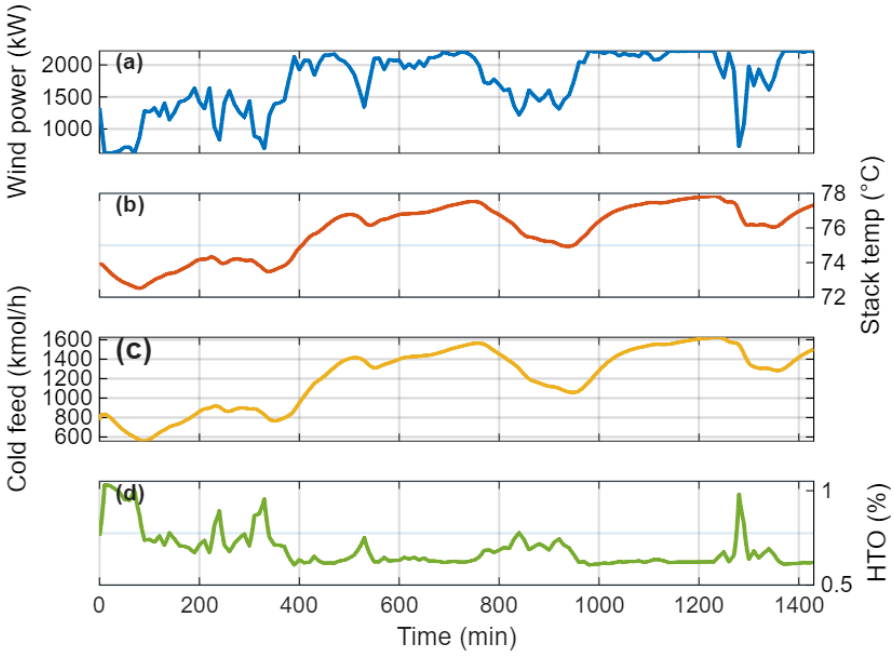

Figure. 8. *Dynamic response of AWE system under high wind power input a) wind power input, b) stack temperature, c) cooling water, d) HTO*

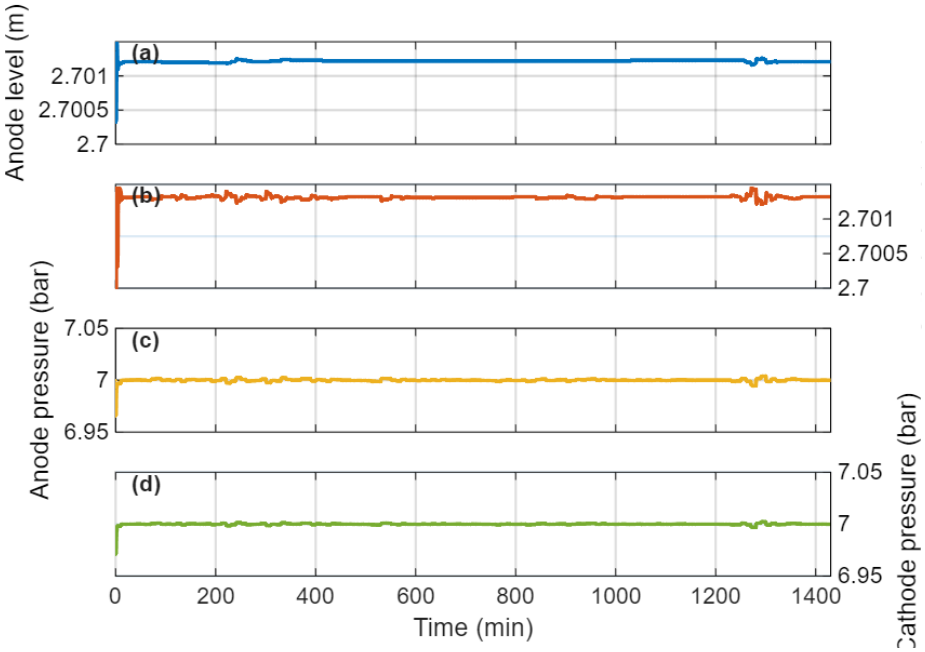

Figure. 9. *AWE separator dynamic under high wind power input a) anode separator level, b) cathode separator level, c) anode separator pressure, d) cathode separator pressure*

4.1.2. Dynamic response under low wind power conditions

A second representative day was selected to investigate system operation under low wind power conditions. The day with the lowest wind power in the annual dataset was not considered, because the available power was insufficient for meaningful hydrogen production. As shown in Figure 10 (a) and (b), the lower power input reduces heat generation in the stack, resulting in a smaller temperature rise. Accordingly, the cooling water flow rate follows the stack temperature trend, as shown in Figure 10 (c). Under this low wind condition, the average wind power was approximately 307 kW, corresponding to about 13% of the load of the AWE system. As shown in Figure 10 (d), the HTO level remained above 1% during operation, which is higher than that observed under high wind power condition but still below the safety threshold. These results clearly demonstrate the importance of defining the operating load range in AWE systems. During this period, a total of 163 kg of hydrogen was produced, corresponding to an average production rate of 6.8 kg/h.

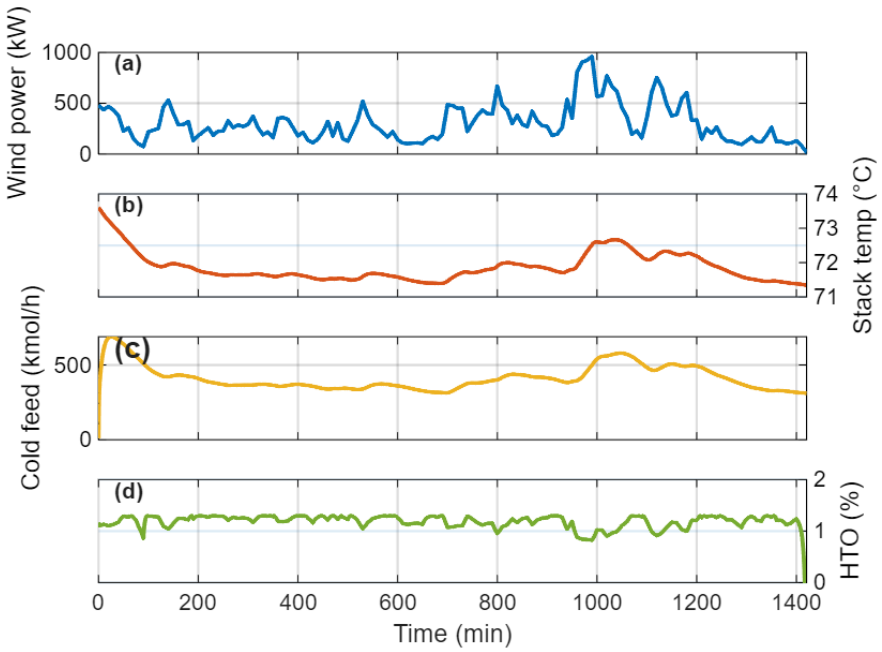

Figure. 10. *Dynamic response of AWE system under low wind power input a) wind power input, b) stack temperature, c) cooling water, d) HTO*

5. Conclusion

This study developed a dynamic model of a MW-scale AWE system to evaluate its performance under fluctuating renewable power input. The model integrates key BOP components, including electrolyte circulation, gas–liquid separation, cooling, and hydrogen purification, enabling system-level dynamic analysis. The thermal analysis demonstrated that the required electrolyte flow is strongly dependent on both operating load and allowable temperature rise, providing a practical guideline for maintaining thermal balance in AWE systems. In addition, the HTO analysis revealed that pressure has a more dominant effect than temperature on gas crossover. The ramp-rate formulation illustrated that rate-of-change constraints can prevent abrupt current-density transitions. The single-bed adsorption results showed that the five-nine hydrogen production duration increased with bed length, providing a preliminary basis for future multi-bed dryer design. Dynamic simulations under wind power input confirmed that the AWE system can maintain stable operation despite significant fluctuations in renewable energy supply. Under high wind conditions, the system operated predominantly at high load, resulting in stable temperature behavior, low HTO levels, and consistent hydrogen production, with a total production of 863 kg/day. In contrast, under low wind conditions, the system operated in the low-load region, where increased gas crossover led to higher HTO levels, although still within the safety limit. The results emphasize the importance of maintaining an appropriate operating load range to ensure safe and efficient operation. Overall, the proposed modeling framework provides a useful tool for analyzing MW-scale AWE systems under renewable-driven conditions. Future work will focus on extending the analysis of low-load operation, where safety constraints become more critical, and on incorporating detailed dynamic modeling of the hydrogen purification process.

Acknowledgments

This work was supported by the Korea Institute of Energy Technology Evaluation and Planning (KETEP) and Ministry of climate, Energy & Environment (MCEE) of the Republic of Korea (No. 00234707).

Appendix A

Table 2. *Electrochemical model for AWE [8].*

Equation	Eq.No.
$$V_{cell} = E_{rev} + V_{act} + V_{ohm}$$	(A.1)
$$E_{rev} = E^0_{rev} + \frac{R_{gas}\,T}{2\,F}\ln\left(\frac{(P_c - P_{sv}(T))\sqrt{(P_a - P_{sv}(T))}}{\alpha_{AWE}}\right)$$	(A.2)
$$V_{act} = \frac{R_{gas}\,T}{F}\sinh^{-1}\left(\frac{i}{\frac{A\,(1-\theta)}{2\,j_{0a}}}\right) + \frac{R_{gas}\,T}{F}sinh^{-1}\left(\frac{i}{\frac{A\,(1-\theta)}{2\,j_{0c}}}\right)$$	(A.3)
$$V_{ohm} = i \cdot \left(R_{anode} + R_{cathode} + R_{separator} + R_{electrolyte}\right)$$	(A.4)
$$\sigma_{Ni\,foam} = \frac{1}{4}\,(1-\beta) * (6 * 10^7) - 279650 * T + 532 * T^2 - 0.38057 * T^3$$	(A.5)
$$\sigma_{KOH} = -204 * m - 0.28 * m^2 + 0.5332 * m * T + 20720 * \frac{m}{T} + 0.1043 * m^3 - 0.00003 * m^2 * T^2$$	(A.6)
$$\sigma_{separator} = \sigma_{KOH} \cdot \frac{\varepsilon}{\tau^2}$$	(A.7)

Appendix B

Table 3. *Electrochemical model parameter*

Category	Variable	Value
Electrode/PTL	Electrode & PTL material	Nickel foam
	Thickness of electrode	1.6 mm
Separator	Separator material	Zirfon Perl UTP 220
	Thickness of separator	220 μm
Electrolyte	Composition	30 wt.% KOH aqueous solution
	Thickness of electrolyte	0.0010295 m

Nomenclature

A	active area	(m^2)
b	water activity	
C_p	specific heat capacity	(kJ kg^{-1} K^{-1})
E_{rev}	reversible voltage	(V)
E_{rev}^0	standard reversible voltage	(V)
F	faraday constant	(C mol^{-1})
i	current	(A)
j	operating current density	(A m^{-2})
m	molar concentration of KOH	
$\dot{m}$	mass flow rate	(kg s^{-1})
P	pressure	(bar)
P_{sv}	vapor pressure	(bar)
R	resistance	(Ω)
R_{gas}	universal gas constant	(J mol^{-1} K^{-1})
T	temperature	(K)
V	voltage or overpotential	(V)

Greek letters

β	mean porosity of nickel foam	
γ	pressure dependency coefficient	
δ	thickness	(m)
ε	porosity of zirfon	
θ	covering rate	
ρ	density	(kg m^{-3})
σ	conductivity	(S m^{-1})
τ	tortuosity of zirfon	
Φ	volume fraction	

Subscripts

a	anode
act	activation
c	cathode
$cell$	cell operating
con	concentration
ohm	ohmic
op	operating
ref	reference
sep	separator

gen	generate
im	impurity

Abbreviation

AWE	Alkaline water electrolysis
MW	Megawatt

References

[1] "Renewable electricity – Renewables 2025 – Analysis," IEA. Accessed: Mar. 31, 2026. [Online]. Available: https://www.iea.org/reports/renewables-2025/renewable-electricity

[2] "John Cockerill's Chinese subsidiary completed the delivery of 24 stacks for the world's largest solar-powered green hydrogen project," John Cockerill. Accessed: Mar. 31, 2026. [Online]. Available: https://johncockerill.com/en/press-and-news/news/john-cockerills-chinese-subsidiary-completed-the-delivery-of-24-stacks-for-the-worlds-largest-solar-powered-green-hydrogen-project/

[3] Y. Wang *et al.*, "Dynamic simulation of wind-powered alkaline water electrolysis system for hydrogen production," *International Journal of Hydrogen Energy*, vol. 97, pp. 391–405, Jan. 2025, doi: 10.1016/j.ijhydene.2024.11.266.

[4] G. Sakas, A. Ibáñez-Rioja, V. Ruuskanen, A. Kosonen, J. Ahola, and O. Bergmann, "Dynamic energy and mass balance model for an industrial alkaline water electrolyzer plant process," *International Journal of Hydrogen Energy*, vol. 47, no. 7, pp. 4328–4345, Jan. 2022, doi: 10.1016/j.ijhydene.2021.11.126.

[5] R. Yin, B. Chen, and L. Sun, "Modelica-based multiphysics modeling and multi-timescale dynamic analysis of a 100-kW alkaline water electrolysis system," *Renewable Energy*, vol. 253, p. 123620, Nov. 2025, doi: 10.1016/j.renene.2025.123620.

[6] M. David, C. Ocampo-Martínez, and R. Sánchez-Peña, "Advances in alkaline water electrolyzers: A review," *Journal of Energy Storage*, vol. 23, pp. 392–403, Jun. 2019, doi: 10.1016/j.est.2019.03.001.

[7] N. Taranin, M. G. Dozein, O. Saborío-Romano, and N. A. Cutululis, "On the Ramp-Rate Limitation of Electrolysis Plants: Modeling Fundamentals and System-Level Impact Analysis," *IEEE Transactions on Sustainable Energy*, vol. 17, no. 2, pp. 1238–1249, Apr. 2026, doi: 10.1109/TSTE.2025.3611711.

[8] S. Lim, S. Im, H. A. Muhammad, J. H. Im, C. Kim, and Y. D. Lee, "Rigorous modeling and wind energy integrated simulation of an alkaline water electrolysis system," *Energy*, vol. 347, p. 140474, Mar. 2026, doi: 10.1016/j.energy.2026.140474.

[9] T. Adibi, A. Sojoudi, and S. C. Saha, "Modeling of thermal performance of a commercial alkaline electrolyzer supplied with various electrical currents," *International Journal of Thermofluids*, vol. 13, p. 100126, Feb. 2022, doi: 10.1016/j.ijft.2021.100126.

[10] Y. Wang *et al.*, "Dynamic simulation of wind-powered alkaline water electrolysis system for hydrogen production," *International Journal of Hydrogen Energy*, vol. 97, pp. 391–405, Jan. 2025, doi: 10.1016/j.ijhydene.2024.11.266.

[11] S. Hu *et al.*, "Analysis of the safe operating boundaries and approaches to expansion in alkaline water electrolysis systems," *International Journal of Hydrogen Energy*, vol. 191, p. 152310, Nov. 2025, doi: 10.1016/j.ijhydene.2025.152310.

[12] M. Sánchez, E. Amores, D. Abad, L. Rodríguez, and C. Clemente-Jul, "Aspen Plus model of an alkaline electrolysis system for hydrogen production," *International Journal of Hydrogen Energy*, vol. 45, no. 7, pp. 3916–3929, Feb. 2020, doi: 10.1016/j.ijhydene.2019.12.027.

[13] H. Lange, A. Klose, L. Beisswenger, D. Erdmann, and L. Urbas, "Modularization approach for large-scale electrolysis systems: a review," *Sustainable Energy Fuels*, vol. 8, no. 6, pp. 1208–1224, Mar. 2024, doi: 10.1039/D3SE01588B.

[14] S. Learman, "VERTICAL GAS-LIQUID SEPARATOR CALCULATOR," 2009.

[15] Y. Ligen, H. Vrubel, and H. Girault, "Energy efficient hydrogen drying and purification for fuel cell vehicles," *International Journal of Hydrogen Energy*, vol. 45, no. 18, pp. 10639–10647, Apr. 2020, doi: 10.1016/j.ijhydene.2020.02.035.

[16] A. Gorbach, M. Stegmaier, and G. Eigenberger, "Measurement and Modeling of Water Vapor Adsorption on Zeolite 4A—Equilibria and Kinetics," *Adsorption*, vol. 10, no. 1, pp. 29–46, Jan. 2004, doi: 10.1023/B:ADSO.0000024033.60103.ff.

[17] M. Simo, C. J. Brown, and V. Hlavacek, "Simulation of pressure swing adsorption in fuel ethanol production process," *Computers & Chemical Engineering*, vol. 32, no. 7, pp. 1635–1649, Jul. 2008, doi: 10.1016/j.compchemeng.2007.07.011.

[18] M. Simo, S. Sivashanmugam, C. J. Brown, and V. Hlavacek, "Adsorption/Desorption of Water and Ethanol on 3A Zeolite in Near-Adiabatic Fixed Bed," *Ind. Eng. Chem. Res.*, vol. 48, no. 20, pp. 9247–9260, Oct. 2009, doi: 10.1021/ie900446v.